Electronic Supplementary Information

Microwave Synthesis of Ultrathin Nickel Hydroxide Nanosheets with Iron Incorporation for Electrocatalytic Water Oxidation

Kaili Yan,[a‡] Meili Sheng,[a‡] Xiaodong Sun,[b,c] Chang Song,[b,c] Zhi Cao,[b,c] Yujie Sun[a*]*

[a]Department of Chemistry, University of Cincinnati, Cincinnati, OH 45221, United States
[b]State Key Laboratory of Coal Conversion, Institute of Coal Chemistry, Chinese Academy of Sciences, Taiyuan 030001, P.R. China
[c]National Energy Center for Coal to Liquids, Synfuels China Co., Ltd, Huairou District, Beijing 101400, P.R. China

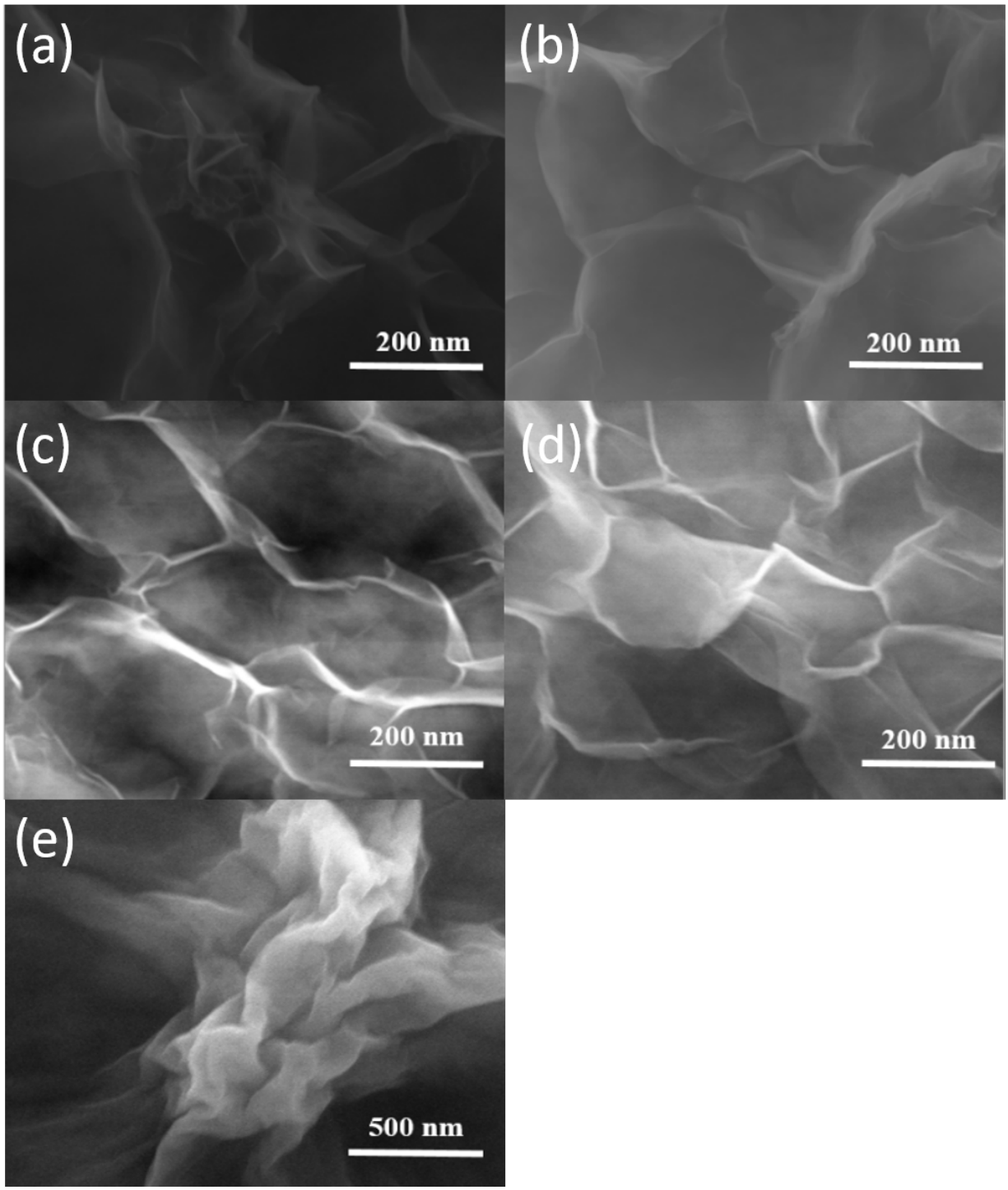

Fig. S1. SEM images of (a) $Ni_{0.99}Fe_{0.01}(OH)_2$, (b) $Ni_{0.95}Fe_{0.05}(OH)_2$, (c) $Ni_{0.89}Fe_{0.11}(OH)_2$, (d) $Ni_{0.84}Fe_{0.14}(OH)_2$, (e) $Ni_{0.71}Fe_{0.29}(OH)_2$.

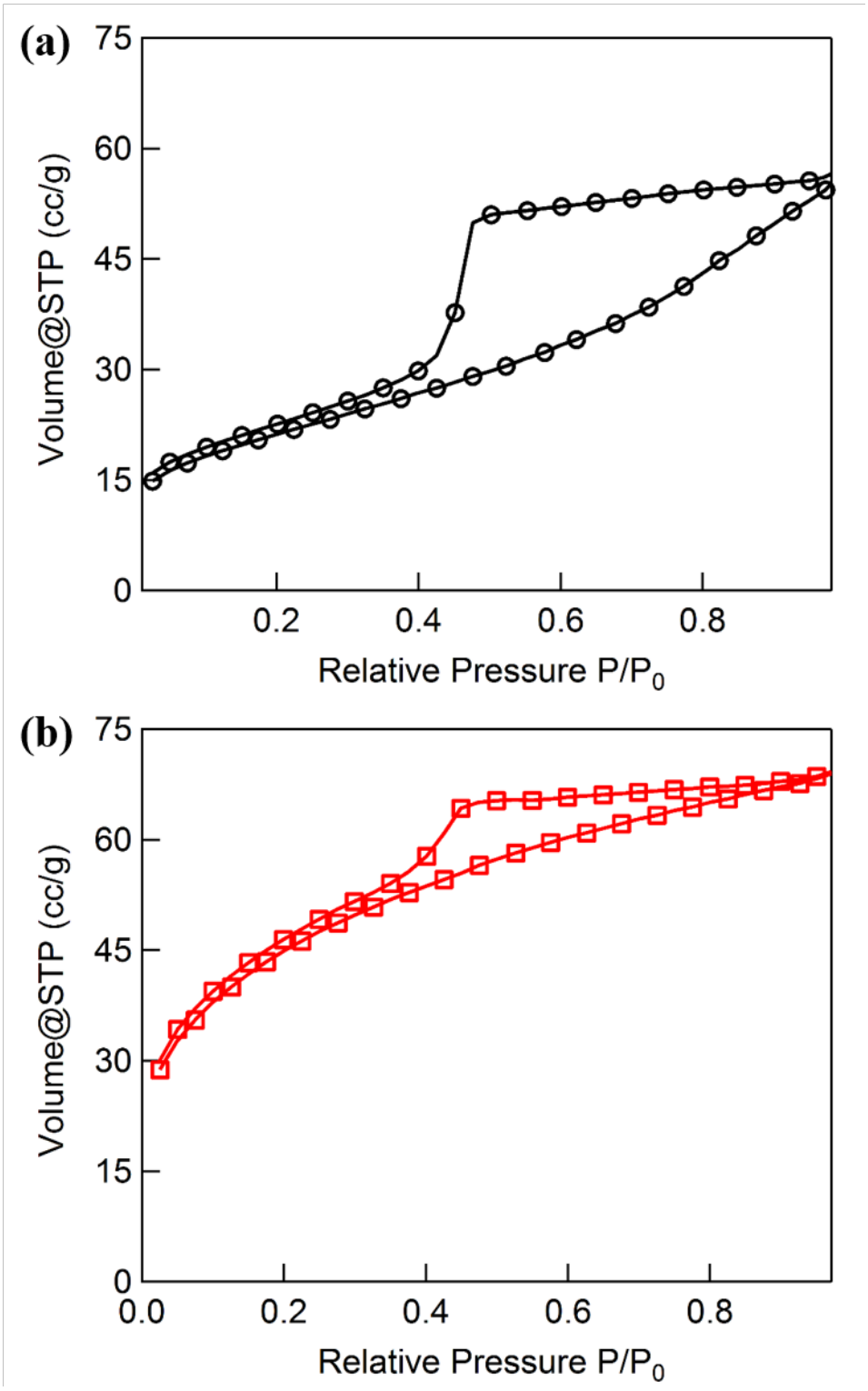

Fig. S2. Nitrogen adsorption-desorption isotherms of $Ni(OH)_2$ (a) and $Ni_{0.78}Fe_{0.22}(OH)_2$ (b).

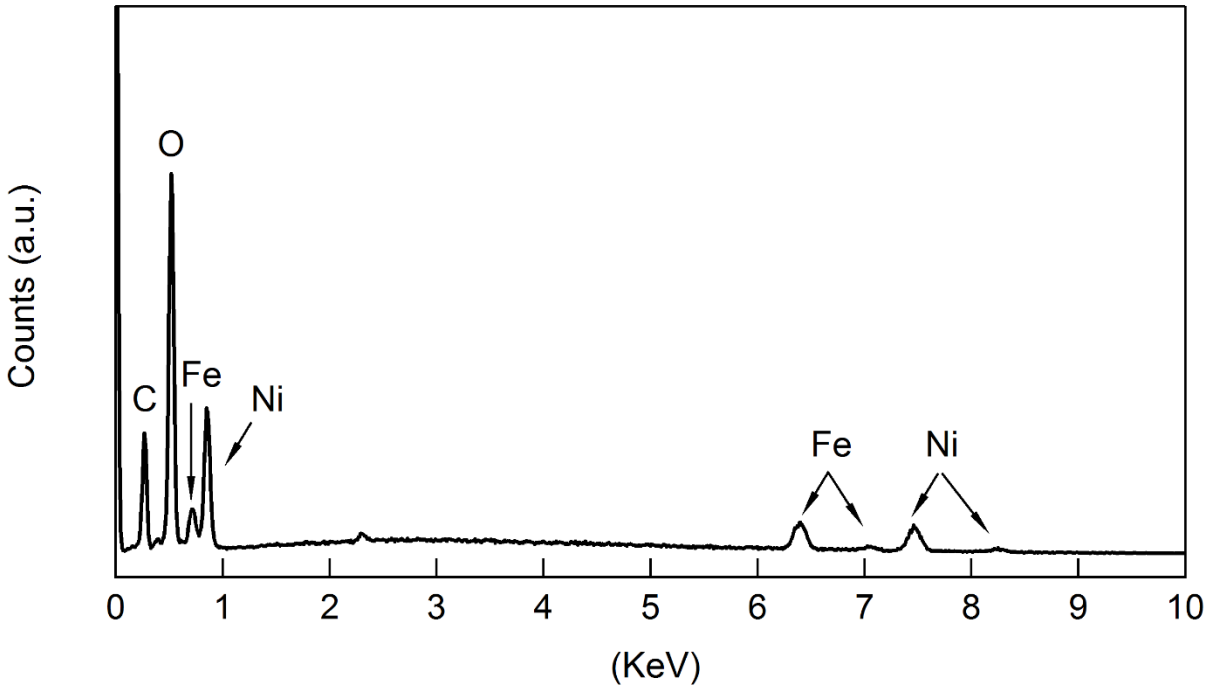

Fig. S3. Energy-dispersive X-ray spectrum of $Ni_{0.78}Fe_{0.22}(OH)_2$.

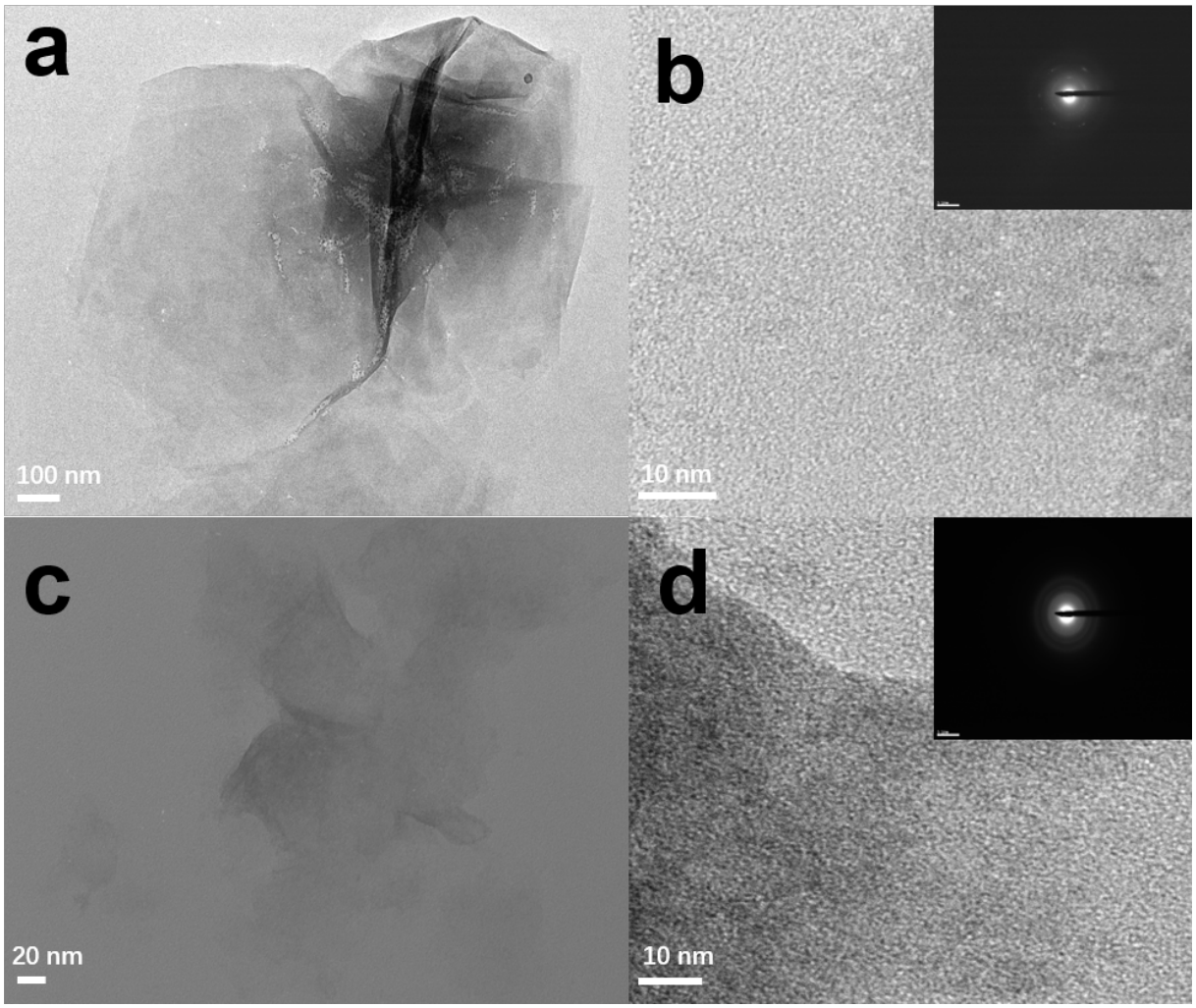

Fig. S4. TEM images of (a-b) $Ni(OH)_2$ (inset is the SAED pattern), (c-d) $Ni_{0.78}Fe_{0.22}(OH)_2$ (inset is the SAED pattern).

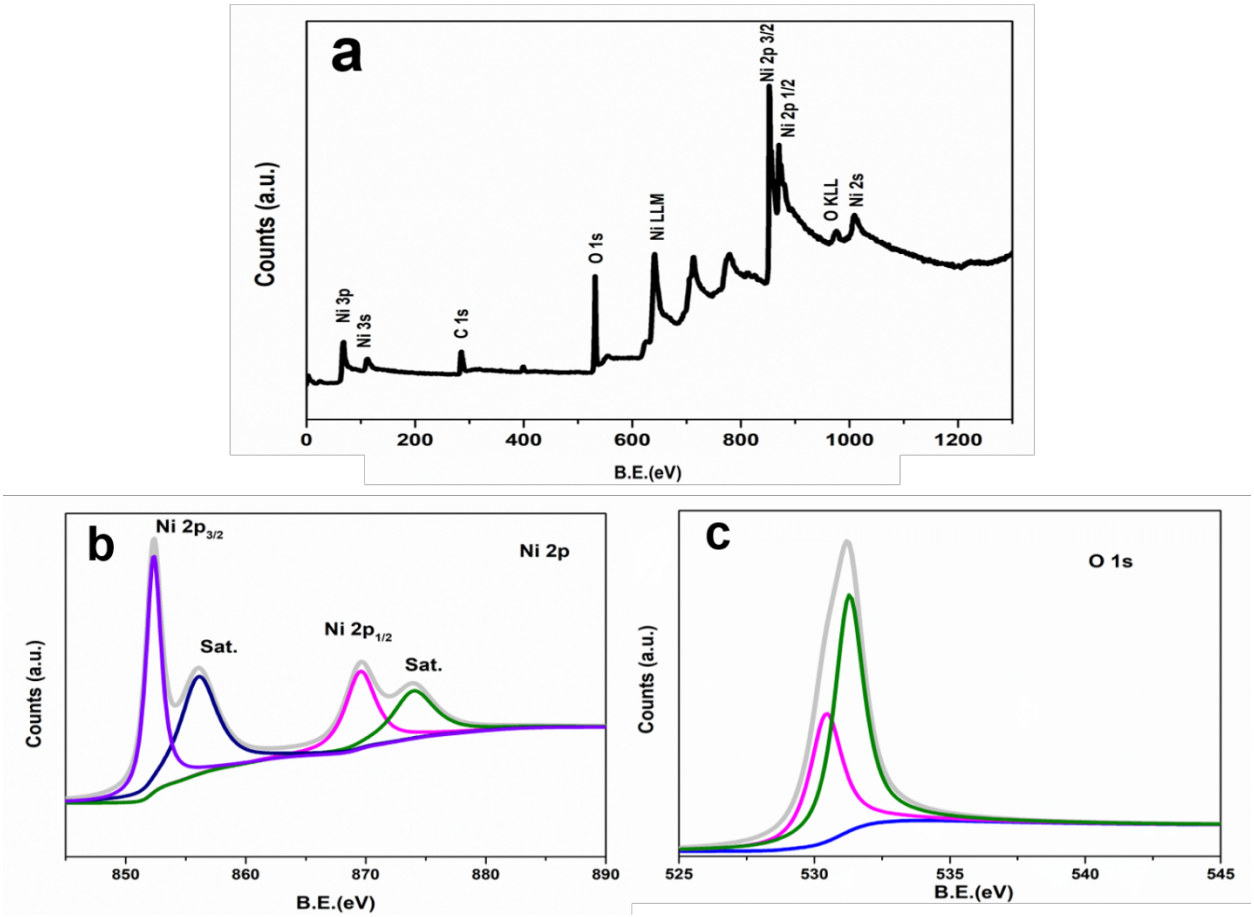

Fig. S5. XPS spectra of $Ni(OH)_2$: survey (a) and the spectral regions of Ni 2p (b) and O 1s (c).

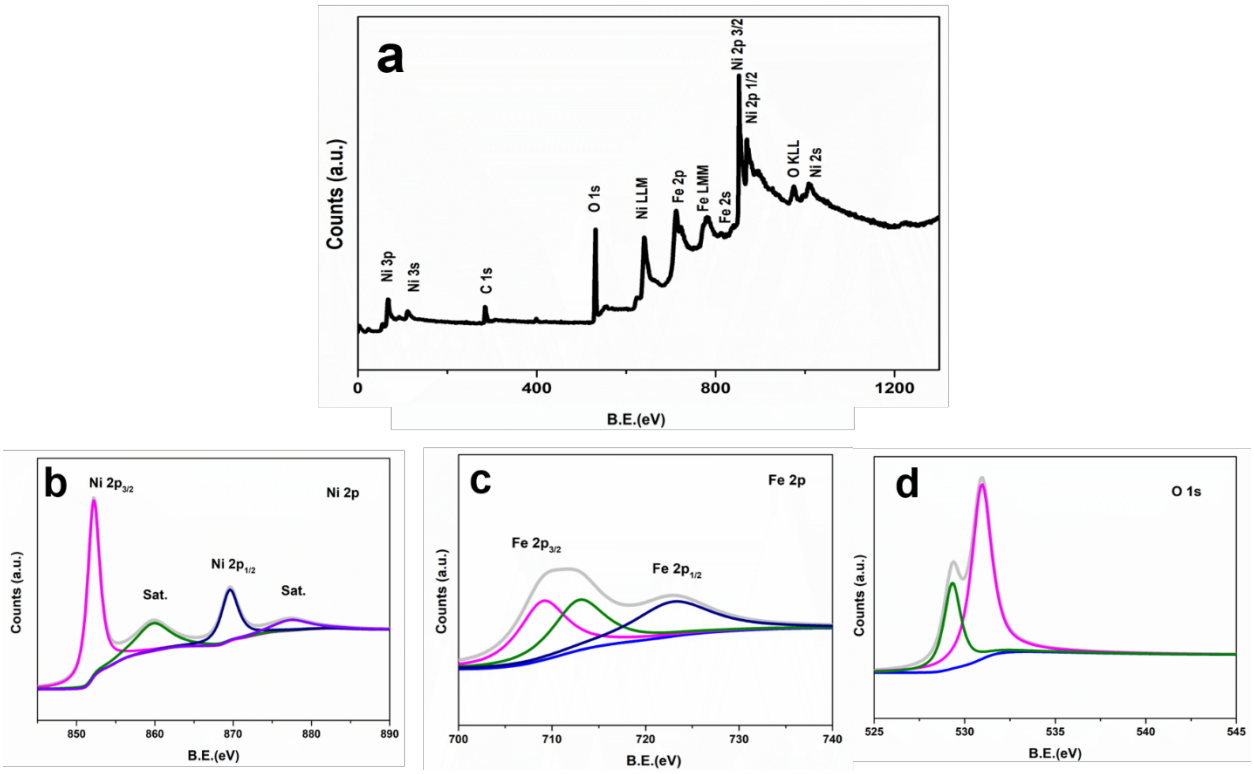

Fig. S6. XPS spectra of $Ni_{0.78}Fe_{0.22}(OH)_2$: survey (a) and the spectral regions of Ni 2p (b), Fe 2p (c) and O 1s (d).

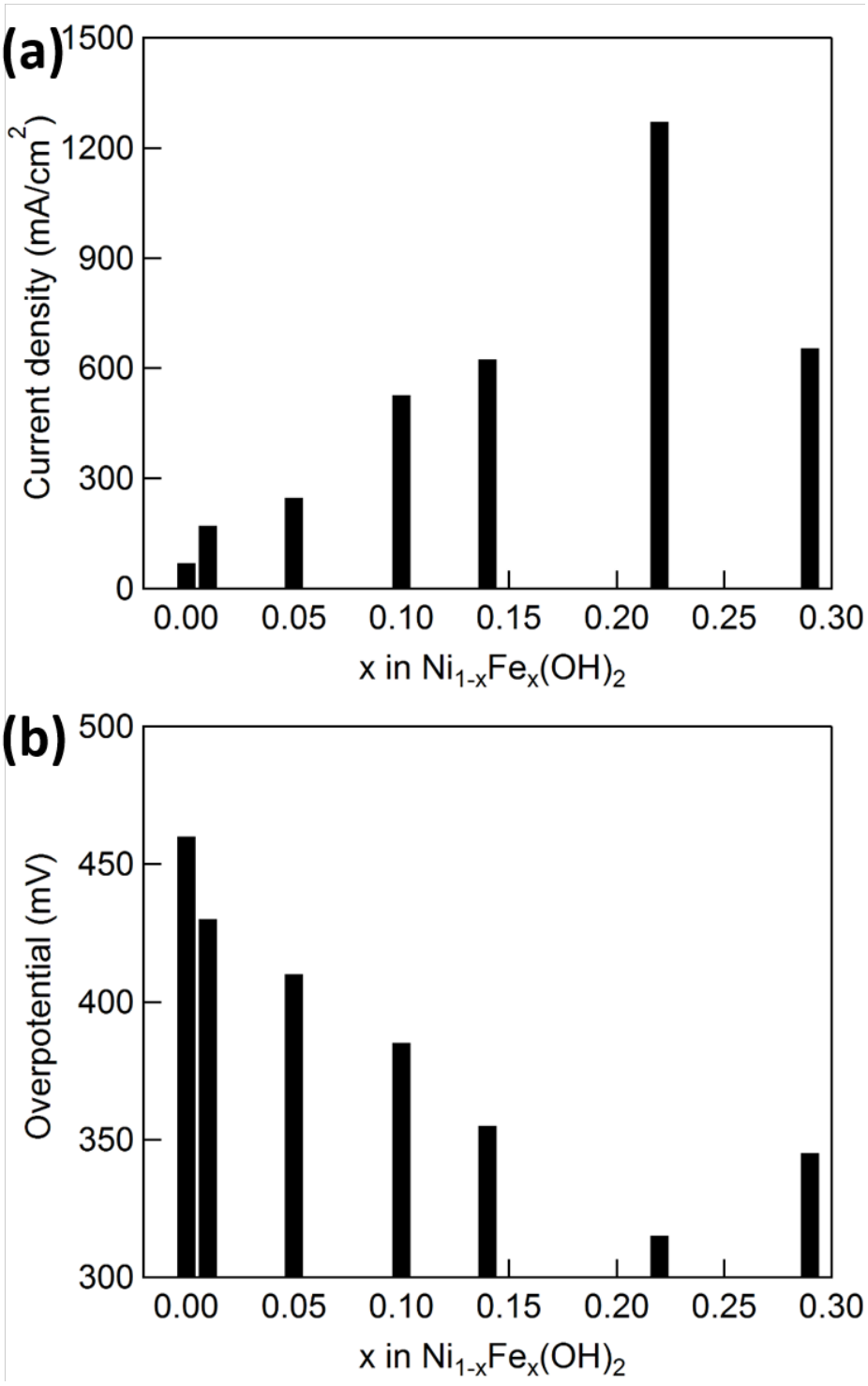

Fig. S7. (a) Current density at 1.8 V vs. RHE. (b) Overpotential at J = 10 mA /cm^2 of $Ni_{1-x}Fe_x(OH)_2$ (x = 0, 0.01, 0.0.5, 0.11, 0.14, 0.22, 0.29) loaded on RDE (2000 rpm) in 1.0 M purified KOH, scan rate = 5 mV/s.

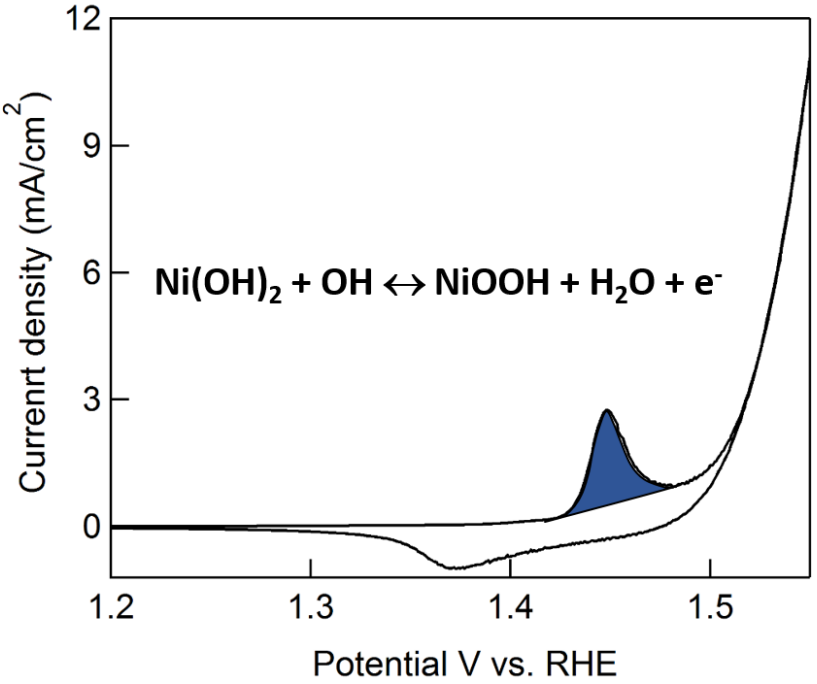

Fig. S8. Cyclic voltammetry of $Ni_{0.78}Fe_{0.22}(OH)_2$ in 1.0 M KOH with scan rate 10 mV/s.

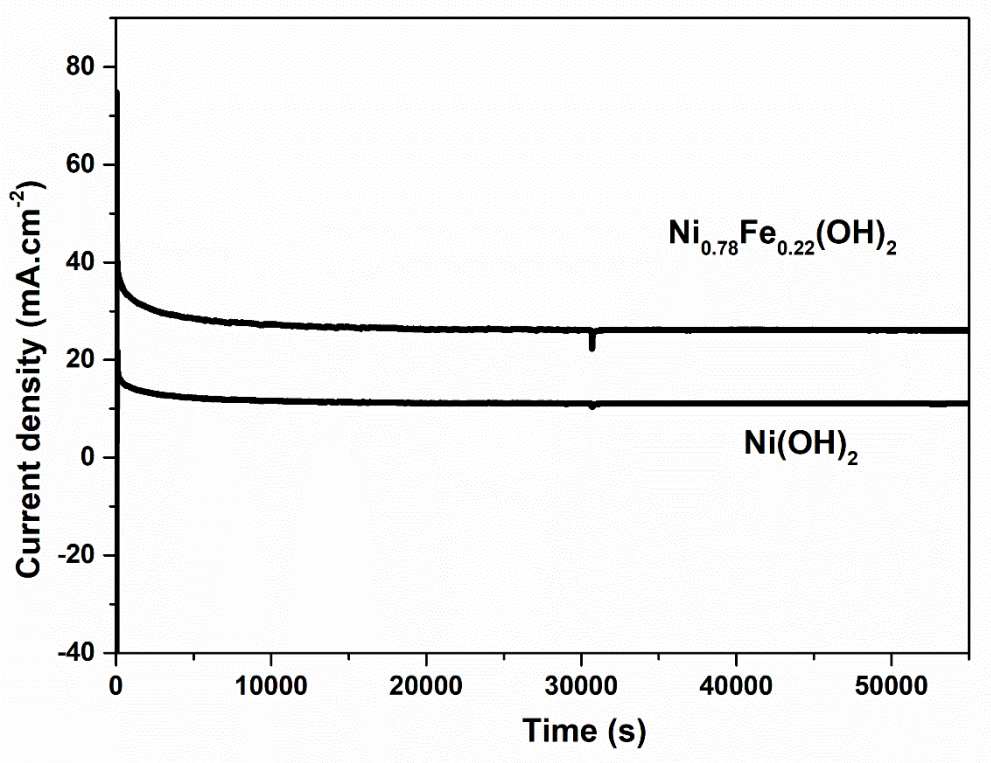

Fig. S9. Chronoamperometric curves of $Ni_{0.78}Fe_{0.22}$ $(OH)_2$ and $Ni(OH)_2$ at 1.54 V (vs. RHE).

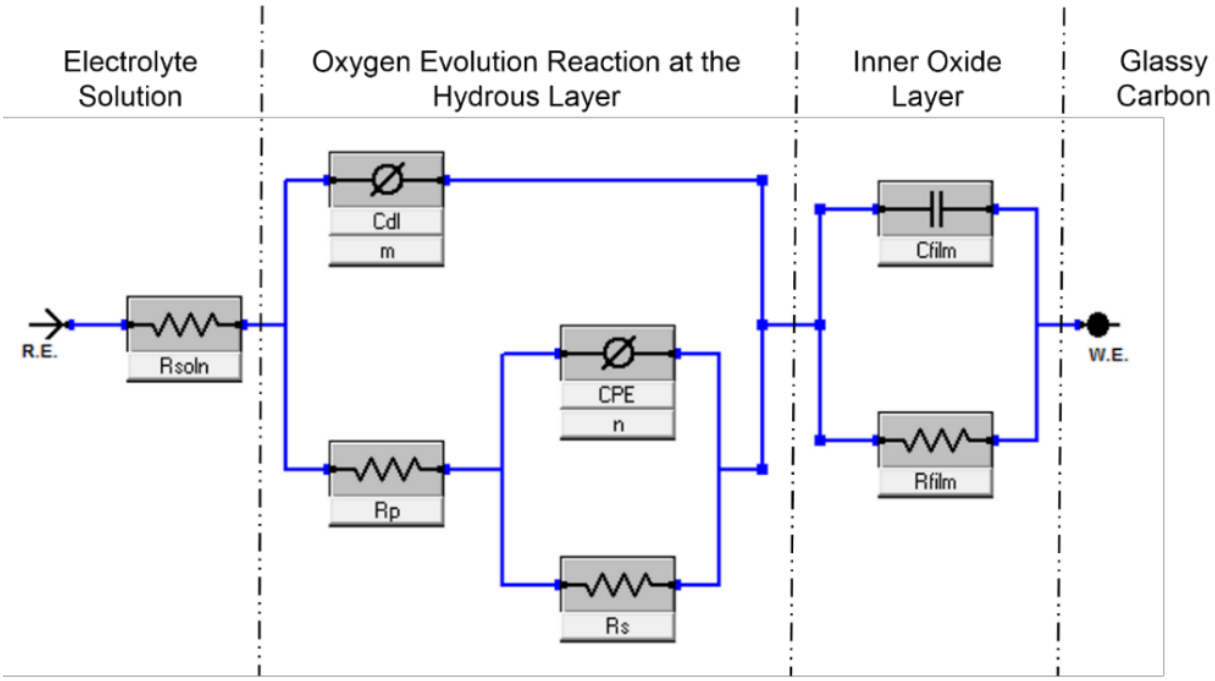

Fig. S10. An electrical equivalent circuit used to model the OER for both $Ni(OH)_2$ and $Ni_{0.78}Fe_{0.22}(OH)_2$. The $C_{film}R_{film}$ loop of the equivalent circuit model is attributed to the dielectric properties and the resistance of the underlying compact oxide film. C_{dl} and R_{soln} represents the double-layer capacitance and electrolyte resistance, respectively. The resistive elements R_s and R_p are related to the kinetics of the interfacial charge transfer reaction; while CPE is given the value of a capacitor.[i,ii]

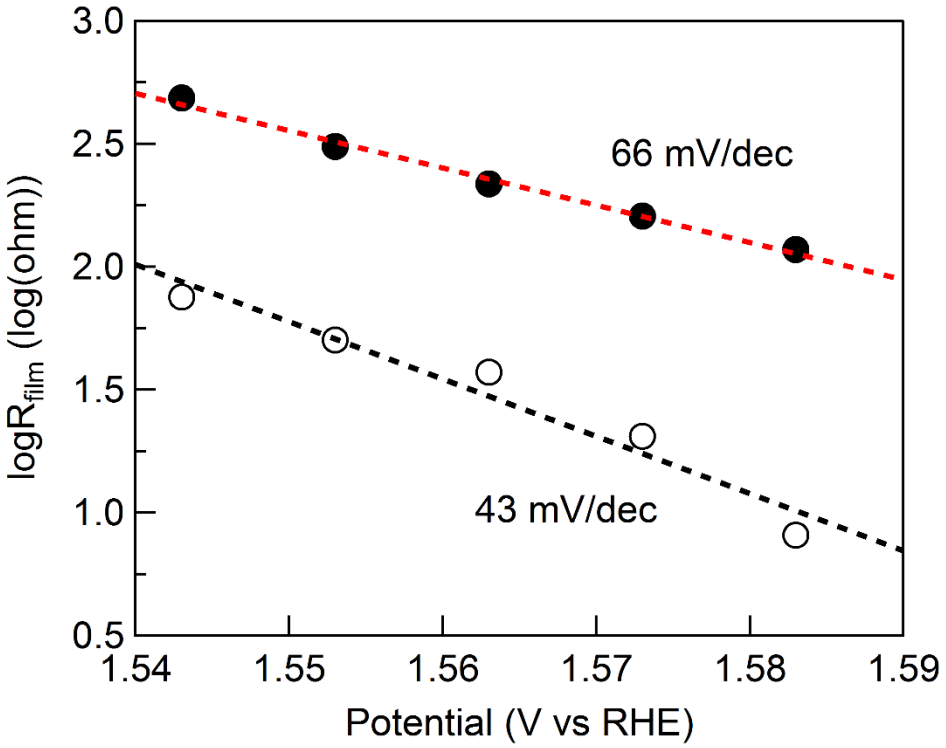

Fig. S11. Catalyst film resistance (R_{film})-based Tafel plots derived from the EIS fitting results of $Ni(OH)_2$ (black) and $Ni_{0.78}Fe_{0.22}(OH)_2$ (white).

Table S1. Original Fe/Ni ratio and the resulting ratio measured via ICP-MS.

Original Fe/Ni ratio	*x* in $Ni_{1-x}Fe_x(OH)_2$
1 : 99	0.01
5 : 95	0.05
10 : 90	0.11
15 : 85	0.14
20 : 80	0.22
30 : 70	0.29

Table S2. The peak ratio of Ni and O in $Ni(OH)_2$ and $Fe_{0.22}Ni_{0.78}(OH)_2$

Electrocatalyst	Ni $2p_{3/2}$/O1s	Ni $2p_{1/2}$/O1s
$Ni(OH)_2$	450000/165000=2.7	360000/165000=2.2
$Fe_{0.22}Ni_{0.78}(OH)_2$	360000/150000=2.4	270000/150000=1.8

Table S3. Integration of anodic and cathodic peak from cyclic voltammetry for $Ni_{1-x}Fe_x(OH)_2$.

x in $Ni_{1-x}Fe_x(OH)_2$	0	0.01	0.05	0.11	0.22	0.29
Integration of anodic peak (mC)	56.6	326.7	278.9	318.7	364.4	64.9
Turnover frequency $(s^{-1})^c$	0.04	0.05	0.06	0.12	0.33	0.33

Table S4. Fitting parameter values of the EIS data for $Ni(OH)_2$

Potential (V)	R_{soln} (Ω)	R_s (Ω)	R_p (Ω)	CPE ($S*s^{-n}$)	n	C_{dl} ($S*s^{-m}$)	m	R_{film} (Ω)	C_{film} (μF)
1.543	9.240	149.8	22.67	9.076×10^{-3}	0.4159	38.65×10^{-6}	0.8476	485.9	1737
1.553	9.304	166.6	21.59	9.820×10^{-3}	0.3767	34.35×10^{-6}	0.8597	309.0	1789
1.563	9.329	117.9	23.54	7.797×10^{-3}	0.3706	33.51×10^{-6}	0.8616	217.4	1848
1.573	9.369	87.28	24.67	6.574×10^{-3}	0.4561	37.42×10^{-6}	0.8511	160.8	1906
1.583	9.446	76.66	28.29	5.293×10^{-3}	0.4659	37.00×10^{-6}	0.8510	117.6	2053

Note: S = siemens, s = second

Table S5. Fitting parameter values of the EIS data for $Ni_{0.78}Fe_{0.22}(OH)_2$

Potential (V)	R_{soln} (Ω)	R_s (Ω)	R_p (Ω)	CPE ($S*s^{-n}$)	n	C_{dl} ($S*s^{-m}$)	m	R_{film} (Ω)	C_{film} (μF)
1.543	10.33	31.89	8.405	3.283×10^{-3}	0.7517	49.71×10^{-6}	0.8544	75.39	1327
1.553	10.46	28.14	8.917	2.912×10^{-3}	0.7596	52.37×10^{-6}	0.8488	50.39	1416
1.563	10.50	20.62	9.037	3.045×10^{-3}	0.7373	49.03×10^{-6}	0.8498	37.30	1355
1.573	10.64	25.00	10.22	1.759×10^{-3}	0.8233	53.05×10^{-6}	0.8364	20.45	2105
1.583	10.36	35.46	10.94	1.048×10^{-3}	0.8953	77.88×10^{-6}	0.7889	8.112	2285

Note: S = siemens, s = second

Table S6. Summary of representative Ni based OER electrocatalysts reported in literature.

Electrocatalysts	Loading (mg/cm^2)	Electrolyte	η_{10} (mV)	Tafel slope (mV/dec)	Ref
$Ni_{0.78}Fe_{0.22}(OH)_2$	0.07	1 M KOH	320	35	This Work
$Ni(OH)_2$	0.07	1 M KOH	470	60	This Work
$PtO–Ni^{2+\delta}O^{\delta}(OH)_{2-\delta}$	-	0.1 M KOH/LiOH	445	-	3
Co-Ni LDH on FTO glass	~0.02	1 M KH_2PO_4	900	230	4
NiCo LDH-4 on Ni foam	-	1 M KOH	419	143	5
Amorphous $Fe_6Ni_{10}O_x$	0.1	1 M KOH	289	48	6
Metallic Ni_3N nanosheets	0.285	1 M KOH	-	45	6
Ni nanoparticles in N doped graphene	0.91	0.1 M KOH	-	188.6	7
Au/mesoporous Co_3O_4	0.1	0.1 M KOH	410	70	7
CoP nanorods/carbon	0.71	1 M KOH	321	71	8
α-$Ni(OH)_2$	0.2	1 M KOH	331	42	9

References:

1. Lyons, M. E; Brandon, M. P. The significance of electrochemical impedance spectra recorded during active oxygen evolution for oxide covered Ni, Co and Fe electrodes in alkaline solution. *J. Electroanal. Chem.*, **2009**, *631*, 62-70.
2. Doyle, R. L.; Lyons, M. E. An electrochemical impedance study of the oxygen evolution reaction at hydrous iron oxide in base. *Phys. Chem. Chem. Phys.*, **2013**, *15*, 5224-5237.
3. Subbaraman, R.; Tripkovic, D.; Chang, K. C.; Strmcnik, D.; Paulikas, A. P.; Hirunsit, P.; Markovic, N. M. Trends in activity for the water electrolyser reactions on 3d M (Ni, Co, Fe, Mn) hydr (oxy) oxide catalysts. *Nat. Mater.*, **2012,** *11*, 550-557.
4. Zhang, Y.; Cui, B.; Zhao, C.; Lin, H.; Li, J. Co–Ni layered double hydroxides for water oxidation in neutral electrolyte. *Phys. Chem. Chem. Phys.*, **2013,** *15*, 7363-7369.
5. Jiang, J.; Zhang, A.; Li, L.; Ai, L. Nickel–cobalt layered double hydroxide nanosheets as high-performance electrocatalyst for oxygen evolution reaction. *J. Power Sources*, **2015,** *278*, 445-451.
6. Kuai, L.; Geng, J.; Chen, C.; Kan, E.; Liu, Y.; Wang, Q.; Geng, B. A Reliable Aerosol-Spray-Assisted Approach to Produce and Optimize Amorphous Metal Oxide Catalysts for Electrochemical Water Splitting. *Angew. Chem. Int. Ed.*, **2014,** *53*, 7547-7551.
7. Chen, S.; Duan, J.; Ran, J.; Jaroniec, M.; Qiao, S. Z. N-doped graphene film-confined nickel nanoparticles as a highly efficient three-dimensional oxygen evolution electrocatalyst. *Energy Environ. Sci.*, **2013,** *6*, 3693-3699.
8. Chang, J.; Xiao, Y.; Xiao, M.; Ge, J.; Liu, C.; Xing, W. Surface oxidized cobalt-phosphide nanorods as an advanced oxygen evolution catalyst in alkaline solution. *ACS Catal.*, ***2015****, 5,* 6874-6878.
9. Gao, M.; Sheng, W.; Zhuang, Z.; Fang, Q.; Gu, S.; Jiang, J.; Yan, Y. Efficient water oxidation using nanostructured α-nickel-hydroxide as an electrocatalyst. *J. Am. Chem. Soc.*, **2014***, 136,* 7077-7084.